Scale Selection and Energy Spectra of Disturbances in Southern Hemisphere Flows

J. S. FREDERIKSEN[1]

National Center for Atmospheric Research,[2] Boulder, CO 80307

(Manuscript received 11 May 1981, in final form 28 July 1981)

ABSTRACT

The growth and nonlinear interaction of initially small-amplitude disturbances, having a complete spectrum of zonal wavenumbers, with zonally averaged flows characteristic of January and May Southern Hemisphere situations, are studied in a multilevel primitive equation spectral model incorporating spherical geometry and viscous dissipation. For January, the fastest growing scale has zonal wavenumber $m = 9$, in close agreement with linear instability theory. However, the contribution from $m = 7$ subsequently exceeds that of $m = 9$ and is largely responsible for the general agreement between model and observed eddy streamfunctions and fluxes. Although the individual wavenumber contributions, e.g., $m = 9$ and $m = 7$ undergo vacillation cycles similar to ones found earlier with single zonal wavenumber disturbances growing on the same zonal flows, the total eddy kinetic energy after the initial growth period is relatively constant. This appears to be due to the interference between the larger number of waves. For May the fastest growing scale has $m = 5$ and initially grows on the polar jet. As the disturbance matures secondary growth occurs on the subtropical jet and the disturbance achieves significant amplitude in the upper troposphere in the latitude band between 30 and 60°. Unlike previous baroclinic instability results, the nonlinear model and observed eddy fluxes are also in close qualitative agreement.

For January a very long-time viscous integration was carried out and the kinetic energy spectra were studied at various stages. When zonal wavenumber $m = 7$ reaches its peak (day 23), the spectrum has an approximate m^{-5} power law. This, however, is not a statistical quasi-steady state and further integration out to days 45–50 was needed to reach such a state. Then it was found that the spectra satisfy the m^{-3} power law of classical two-dimensional and quasi-geostrophic turbulence theory.

1. Introduction

The growth of small-amplitude disturbances in Southern Hemisphere zonally averaged flow recently has been examined (Frederiksen, 1981a,b, hereafter referred to as F1 and F2, respectively) in multilevel models incorporating spherical geometry. In F1, the growth rates, phase speeds, perturbation streamfunctions and eddy momentum and heat fluxes were obtained using a quasi-geostrophic baroclinic instability model for different months (January, May and August). In F2, we studied how nonlinear, non-geostrophic, viscous and topographic effects modified the results for January and May flows using a primitive equation model in which the disturbances had a single zonal wavenumber (and harmonics generated through nonlinear interactions).

In this article we complete our study of disturbances growing on Southern Hemisphere (zonally averaged) flows by considering disturbances which have contributions from all zonal wavenumbers. This makes it possible to study the scale selection mechanism which determines which zonal wavenumber m will be dominant during the initial approximately exponential growth period. Furthermore, it allows us to study how the vacillation cycles found in F2 are modified when there is a complete spectrum of waves interacting.

The numerical simulations are carried out in a nine-level primitive equation spectral model without diabatic heating or moist processes and the methodology is similar to that of Gall *et al.* (1979) for Northern Hemisphere flows. However, apart from the application of the present results to understanding Southern Hemisphere dynamics, our findings differ in several important ways from the above study. In particular, for January the integration is carried out for considerably longer and it is found that while at day 23 an approximately m^{-5} spectrum is obtained for the kinetic energy, this is not a statistical quasi-steady-state spectrum and that near the end of the integration (days 45–50) an m^{-3} spectrum is obtained. Thus our results are consistent with the classical theories of two-dimensional and quasi-geostrophic turbulence (Kraichnan, 1967; Charney, 1971).

We also find that, while for the January flow case the fastest growing scale is $m = 9$, the scale with zonal wavenumber $m = 7$ eventually exceeds that of

[1] Permanent affiliation: CSIRO, Division of Atmospheric Physics, Station Street, Aspendale, Victoria, Australia 3195.

[2] The National Center for Atmospheric Research is sponsored by the National Science Foundation.

0022-4928/81/122573-12$07.00
© 1982 American Meteorological Society

Unauthenticated | Downloaded 02/23/24 11:48 PM UTC

$m = 9$ and makes the most important contribution to the disturbance and eddy fluxes. For the May flow, the presence of two distinct jets complicates the evolution of the disturbance. Here the disturbance initially starts growing on the polar jet but near the peak of the energy cycle it spreads and continues to grow on the subtropical jet, yielding disturbance structures and eddy fluxes in qualitative agreement with observations.

In Sections 2 and 3 we discuss the primitive equation spectral model used and the initial conditions. In Section 4 the growth and nonlinear development of the eddy kinetic energy during the simulations are examined. In Sections 5 and 6 we study the time variations of wave amplitudes, eddy momentum and heat fluxes, mean zonal winds and temperature for January and May. Section 7 contains an analysis of the kinetic energy spectra at critical stages in the evolution of the January flow. The conclusions are summarized in Section 8.

2. The primitive equation model

For this study the spherical primitive equation spectral model developed by Bourke (1974) and Bourke *et al.* (1977) has been used, with the parameterizations of vertical and horizontal diffusion as described in Eqs. (2.8) to (2.12) of F2. In particular the horizontal diffusion is described essentially by a $K_h\nabla^2$ (plus constant) operator where

$$K_h = 2.5 \times 10^5 \text{ m}^2 \text{ s}^{-1}. \qquad (2.1)$$

The vertical diffusion, which plays a less important role, is as given in Eqs. (2.11) and (2.12) of F2.

The fields are represented by nine levels (given in Table 1 of F2) in the vertical using the sigma-coordinate system and by spherical harmonics in the horizontal. A rhomboidal truncation of the fields is employed with a rhomboidal truncation wavenumber $J = 21$. A semi-implicit time integration scheme is used with a time step of 40 min for January and 30 min for May.

3. Initial conditions

The initial conditions from which the numerical integrations are begun consist of January and May zonal flows together with small-amplitude disturbances which have nonzero contributions for all zonal wavenumbers $m \neq 0$.

a. The zonal mean flow profiles

The same zonal mean basic states described in F2 are used here. Thus the mean zonal winds for January and May are shown in Figs. 1a and 1c of F1 while the zonal mean temperatures are given in Figs. 1a and 1b of F2. The vertical coordinate σ in these diagrams is related to the pressure through the relation $\sigma = p/p_*$, where $p_*(\lambda, \mu)$ is the surface pressure. For the initial conditions the $m \neq 0$ components of $p_*(\lambda, \mu)$ are set to zero. Again, for January the effects of topography are neglected (except for an extrapolation of the fields to sea level) but for May zonally averaged topography is included in the model in the manner described in Section of F2. For January the divergence amplitudes are set to zero while for May the divergence amplitudes are determined through a normal mode initialization procedure (Machenhauer, 1977; Daley and Puri, 1980) which produces a smooth start.

b. The small-amplitude disturbances

The small-amplitude perturbations with $m \neq 0$ are obtained from the original three-dimensional streamfunction and temperature fields for January and May described in F1 by rescaling their amplitudes such that the total eddy kinetic energy per unit mass is $\sim 10^{-3}$ m^2 s^{-2}; the exact values are shown on the diagrams of kinetic energy in Fig. 1. For both January and May, the perturbation divergence amplitudes and surface pressures are set to zero.

Throughout this article we concentrate on the new aspects of the behavior of the eddies which differ from the results of F2 (and F1). Further references to the literature also may be found in F1 and F2.

4. Growth of eddy kinetic energy

Here we study the changes in the eddy kinetic energy during the evolution of the disturbances.

a. January flow

Fig. 1a shows the change in the total eddy kinetic energy during the integration (bold solid line) and also the kinetic energy of the first odd zonal wavenumbers up to $m = 9$, which turn out to contain the first two, fastest growing components $m = 9$ and $m = 7$. The caption to Fig. 1a describes the types of lines used for the different zonal wavenumbers. We notice that while the total eddy kinetic energy remains fairly constant after day 22, the individual zonal wavenumber contributions, particularly $m = 9$ and $m = 7$, undergo vacillations similar to those in F2 but with a longer period. In fact, after day 25, the energies of the individual wavenumbers are only plotted every five days, tending to smooth out the vacillations.

We see that during the period of almost exponential growth the zonal wavenumber $m = 9$ makes the largest contribution to the energy and amplitude of the disturbance. Thus, for this particular flow, baroclinic instability theory is close to being correct in predicting $m = 10$ as the fastest growing mode. It is expected that the presence of viscous and non-

Unauthenticated | Downloaded 02/23/24 11:48 PM UTC

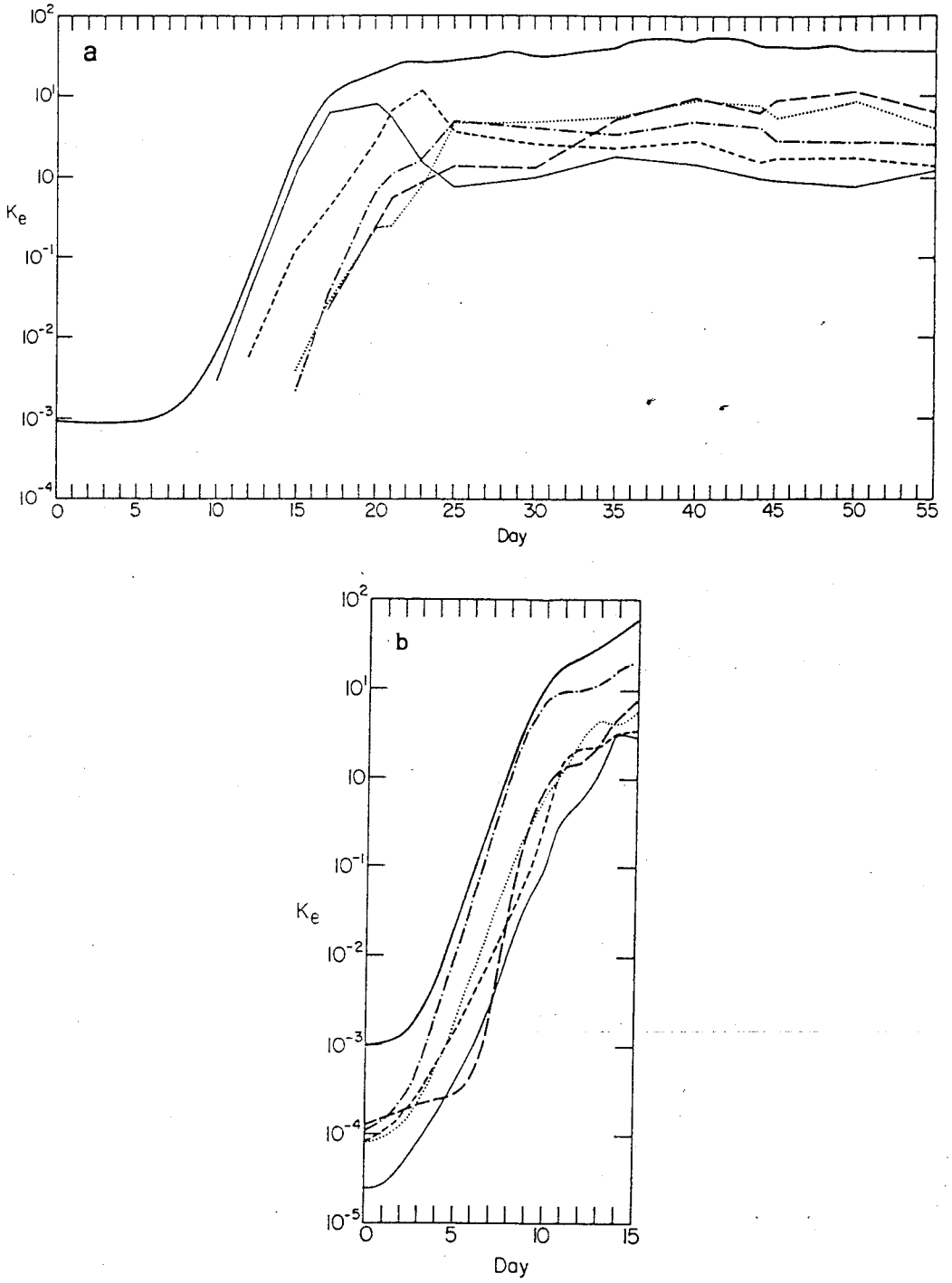

FIG. 1. Time variation of the eddy kinetic energy per unit mass in $m^2\ s^{-2}$ (averaged over the model atmosphere) growing on (a) the January and (b) the May zonal mean state. Curves shown are the total kinetic energy (bold solid) and as well the contributions from the waves with odd zonal wavenumbers $m = 9$ (light solid), $m = 7$ (short-dashed), $m = 5$ (dash-dot), $m = 3$ (dotted) and $m = 1$ (long-dashed). For January, the integration is inviscid between days 50 and 55.

linear effects will move the wavenumber of the most significant mode to lower wavenumbers; in the present case the wavenumber is only decreased by one.

If we use the formula (4.1) of F2 for calculating the growth rate during the period of initial exponential growth, then we find that the growth rate is slightly larger than the largest in Fig. 3a of F1. This is consistent with the findings of differences of

Unauthenticated | Downloaded 02/23/24 11:48 PM UTC

growth rates in primitive equation and quasi-geostrophic models (Simmons and Hoskins, 1976, F2).

Although zonal wavenumber $m = 9$ is the wavenumber which first reaches significant amplitude, $m = 7$ subsequently reaches an even larger amplitude. Thereafter, increasingly smaller zonal wavenumbers come to dominate the kinetic energy until at day 50 the total kinetic energy spectrum is practically a monotonic decreasing function of zonal wavenumber. After day 50 the viscous terms were removed and the model integrated for a further five days. A detailed discussion of the viscous and inviscid spectra will be given in Section 7.

b. *May flow*

For May the change in the eddy kinetic energy during the integration is shown in Fig. 1b. The total kinetic energy is depicted by the bold solid curve and the diagram also shows the contribution from the first odd zonal wavenumbers up to $m = 9$; the types of curves used for the different wavenumbers are described in the caption. It turns out that after the first few days the contribution from zonal wavenumber $m = 5$ is the fastest growing and dominates the kinetic energy during the integration period of 15 days. Again, during the period of almost exponential growth the growth rate as calculated by Eq. (4.1) of F2 is somewhat larger than the corresponding linear quasi-geostrophic growth rate.

For May, the dominant wavenumber $m = 5$ in the nonlinear calculation is considerably different from the fastest growing wave with $m = 10$ in the linear calculation of F1. This is in contrast to the January results where the $m = 9$ dominant wavenumber in the nonlinear calculation compares closely with the fastest growing mode of linear theory (having $m = 10$). Presumably, the differences between the two cases may be attributed to the fact that for May the relative difference between the linear growth rates of waves with $m = 5$ and $m = 10$ is considerably less than for January. Thus, it would seem that it would be easier to move the dominant wavenumber to $m = 5$ for the May case in the presence of viscous damping and nonlinear effects.

Comparing Figs. 1a and 1b we see that the ratio of the maximum eddy kinetic energy for May to that for January is perhaps slightly too large compared with observations. This may be partly due to the fact that the January basic-state zonal flow has been obtained from monthly averages from 1972 to 1976 while the May basic-state zonal flow was taken from the "instantaneous" flow for 19 May 1979. It must also be kept in mind that the model does not contain all the physical mechanisms of general circulation models (cf. McAvaney *et al.*, 1978, and references therein) and in particular the zonal flow is not restored toward its initial values. This, of course, must be kept in mind when interpreting the long-time behavior of the spectra in Fig. 1a.

5. Results for January growth period

a. *Disturbance streamfunctions*

During the first eight or nine days the initial perturbation rearranges its structure. By day 10 the disturbance is dominated by the wavenumber $m = 9$ contribution which has a structure very similar to that shown in Fig. 6a of F1 for the $m = 10$ perturbation. From then until day 20 the qualitative changes in the structure of the dominant wavenumber $m = 9$ contribution is very similar to that described in F2 for the $m = 10$ disturbance growing on the January zonal flow during the first 10 days of its evolution. In particular, as the wave grows and occludes, there is a relative increase in the amplitude at $\sigma = 0.5$ although at no stage does it exceed that at the surface. Fig. 2a shows the contribution to the wave amplitude from $m = 9$ at day 20.

Between days 20 and 22, the wave amplitude changes from being dominated by $m = 9$ to having largest contribution with $m = 7$. The amplitude of the $m = 7$ contribution at day 22 is shown in Fig. 2b. At this stage the wave has largest amplitude in the upper troposphere ($\sigma = 0.4$) and a structure which is very similar to that shown in Fig. 6c of F2 for the $m = 7$ wave at day 13 growing on the January zonal flow. During the next two days the surface minimum of wave amplitude moves poleward to being centered on latitude 50° and the wave decreases its upper level minimum (to 7.65×10^5 m^2 s^{-1}). Thereafter there are further changes in the wavenumber which makes largest contribution to the streamfunction and its kinetic energy as shown in Fig. 1a.

It was discussed in F2 that it is not a simple matter to decide what averaging period would be suitable for comparing model results with observations since this period should be determined by processes such as radiation, convection and release of latent heat which tend to restore the zonal mean flow toward its original strength but which are not included in the present model. However, it would seem that in order for the model results to reproduce upper level maxima of eddy quantities, such as that in the standard deviation of the meridional wind for December–February in Table 3.6 of Newell *et al.* (1972), one would need to include the period between days 21 and 24, where $m = 7$ dominates the wave amplitude. Thus we have here an example of a case where the fastest growing $m = 9$ wave initially dominates the spectrum and wave amplitudes but the second fastest growing $m = 7$ wave subsequently reaches larger amplitude and makes the most important contribu-

Unauthenticated | Downloaded 02/23/24 11:48 PM UTC

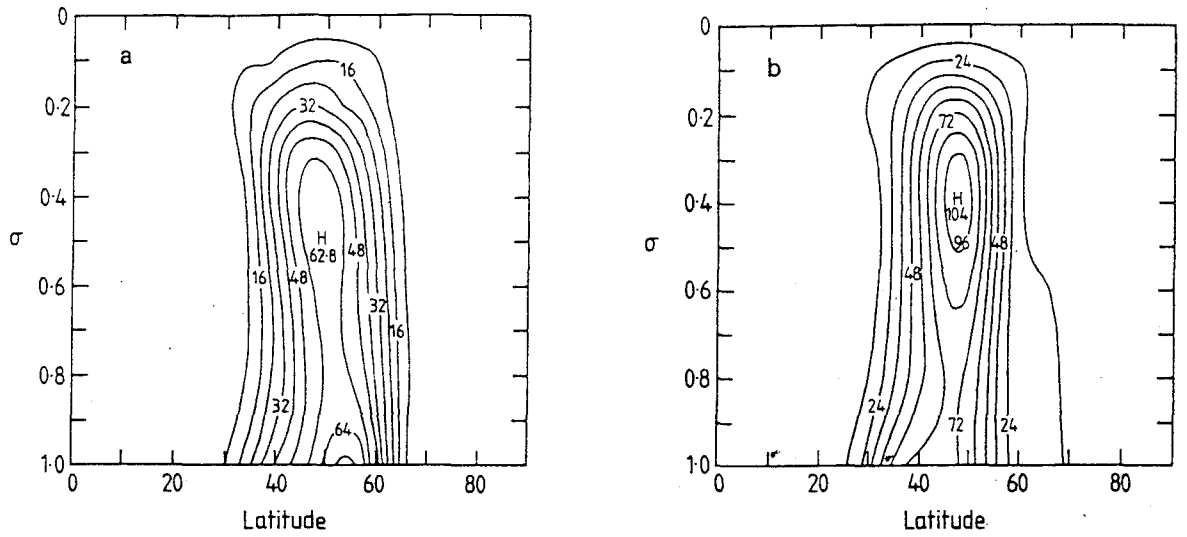

FIG. 2. Contribution to eddy streamfunction amplitude growing on the January zonal mean state from (a) $m = 9$ at day 20 and (b) $m = 7$ at day 22. The units shown correspond to 10^4 m^2 s^{-1}.

tion. Eventually, the spectrum becomes practically monotonically decreasing, but it seems safe to assume that before this could happen in the atmosphere, radiative, convective and moist processes would take over.

b. Eddy momentum fluxes

By day 10, when the disturbance amplitude is dominated by $m = 9$, the eddy momentum flux is largely poleward, centered on 46° latitude and concentrated in the lower troposphere. It has an appearance very similar to that obtained from the instability analysis in F1 for the $m = 10$ disturbance growing on the January zonal flow and which is shown in Fig. 8 of F1; as depicted there the equatorward component is small. Subsequently, the upper-level amplitudes of both the poleward and equatorward fluxes increase relative to those at the surface until by day 18 the maximum poleward flux is centered at $\sigma = 0.5$ and 46° latitude (with magnitude 14.1 m^2 s^{-2}) while the corresponding equatorward flux is centered at $\sigma = 0.45$ and 56° latitude (with magnitude 3.02 m^2 s^{-2}). Thereafter, the surface and the equatorward fluxes decrease until at day 20 the momentum flux has the structure shown in Fig. 3a.

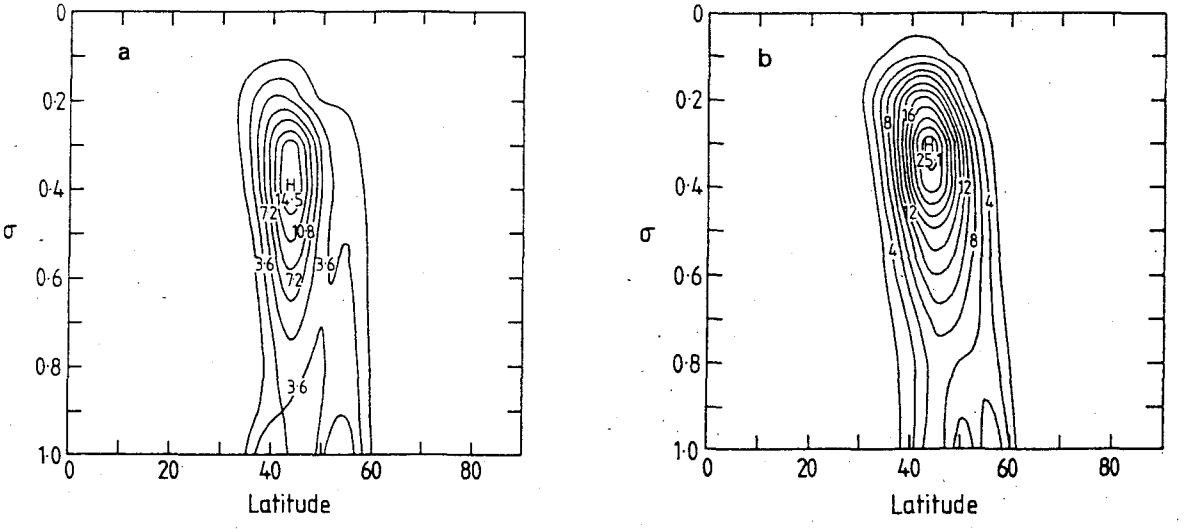

FIG. 3. Contribution to the zonally averaged eddy momentum flux by the rotational component of the wind $\overline{u_r v_r} \cos^2\phi$ in m^2 s^{-2} from (a) $m = 9$ at day 20 and (b) $m = 7$ at day 24 for January.

Unauthenticated | Downloaded 02/23/24 11:48 PM UTC

As the wave amplitude comes to be dominated by $m = 7$, the upper level momentum flux becomes stronger and its center penetrates further into the upper troposphere as shown in Fig. 3b at day 24. We notice that the structure near the peak of the energy cycle resembles closely that found in F2 with the single wavenumber $m = 7$ (plus harmonics) wave growing on the January zonal flow. The maximum flux obtained here (of 30.8 m^2 s^{-2} at day 23) is less than that of F2 and somewhat weaker than the observations for December to February shown in Fig. 4.9 of Newell *et al.* (1972).

c. Eddy heat fluxes

On day 10, the poleward heat flux of the growing wave which is dominated by $m = 9$, closely resembles that shown in Fig. 9 of F1 for the $m = 10$ disturbance growing on the same jet. Thereafter, until day 20, the heat flux penetrates increasingly into the troposphere, but throughout the largest heat flux occurs at the surface. Between days 20 and 22, the wave comes to be dominated by wavenumber 7, and thereafter a distinct secondary maximum occurs centered on $\sigma = 0.5$ and 45° latitude. On day 24, the heat flux in the upper troposphere has a maximum of 6.35 K m s^{-1} and is nearly equal to the lower tropospheric maximum (of 6.55 K m s^{-1}). At this stage the qualitative structure of the heat flux is similar to that shown in Fig. 8c of F2.

Comparing these results with those in Table 7.2 of Newell *et al.* (1974) for December to February, we see that they are a considerable improvement over the linear results of F1, but are somewhat too weak in relation to the observations. Note, however, that the observations also contain contributions from the standing eddies.

d. Changes in the mean zonal wind

During the integration the zonal mean wind in the lower layers increases from that shown in Fig. 1a of F1 to being a large fraction of the maximum zonal wind at the lower levels at the latitude of the jet center. For example, at day 20, the maximum zonal mean wind occurs at $\sigma = 0.336$ and 50° latitude and is 34.6 m s^{-1} while even at the lowest level of $\sigma = 0.991$ it is 18.9 m s^{-1}. Thus the vertical shear is considerably decreased from the initial mean state. For the first 22 days the zonal mean wind increases gradually to a maximum of ~35 m s^{-1}. Thereafter, as both wavenumber 7 and 9 contributions to the wave decay there is a sudden increase of the wind maximum to 38 m s^{-1} at day 25 and a further gradual increase to 41.5 m s^{-1} by day 27. Subsequently, the zonal wind maximum undergoes gradual oscillations until the end of the integration period.

e. Temperature changes

The temperature changes that occur during the first 27 or so days of the integration are qualitatively quite similar to those described for the January integrations in F2 and shown in Fig. 10 and Table 1 of F2 except that the vacillation cycle is less noticeable. In particular the temperature difference between 55 and 40° latitude at the lowest level of $\sigma = 0.991$ changes from 11.8 K at day 0 to 3.2 K at day 22 and back to 7.8 K at day 27.

6. Results for May

a. Disturbance streamfunctions

By day 6 when the perturbation kinetic energy is dominated by zonal wavenumber $m = 5$ (cf. Fig. 1b), the disturbance streamfunction is centered on 70° latitude and has maximum amplitude at the surface. In fact, it has a structure which is very similar to that of mode A with $m = 5$ obtained in the linear model in F1. This shows that even in the presence of viscous and topographic effects, mode A which grows on the polar jet is the fastest growing. During the integration the ratio of the mid-tropospheric to surface amplitudes increases until at days 11 and 15 the perturbations have the appearance shown in Figs. 4a and 4b. At day 11 the $\sigma = 0.5$ and surface maximum amplitudes are practically equal and we see a slight equatorward movement of the center and the beginning of a secondary region of growth at 40° latitude. That is, the perturbation appears to be starting to grow on the subtropical jet. Fig. 1b shows a secondary period of growth from day 11 onward. This appears to be largely due to growth on the subtropical jet with little change in the part of the disturbance which was growing on the polar jet as shown for day 15 in Fig. 4b.

As indicated above, the linear study of F1 correctly predicts the structure of the initial exponentially growing disturbance (centered in a narrow band about 70° latitude) in the nonlinear integration even in the presence of topography and viscosity. However, the subsequent nonlinear modification is such that, by day 15 when the streamfunction has two maxima near $\sigma = 0.4$ and 37 and 57° latitude, it bears little resemblance to the initial disturbance. In fact, due to the presence of the two jets, the amplitude at day 15 differs from linear results not only in the usual way of additional upper level amplification but also in having a more complicated structure. At this stage of the integration the structure of the wave amplitude with maxima in the upper troposphere compares reasonably well with the observations as deduced, for example, from the standard deviation of the meridional wind for March to May given in Table 3.6 of Newell *et al.* (1972). We

Unauthenticated | Downloaded 02/23/24 11:48 PM UTC

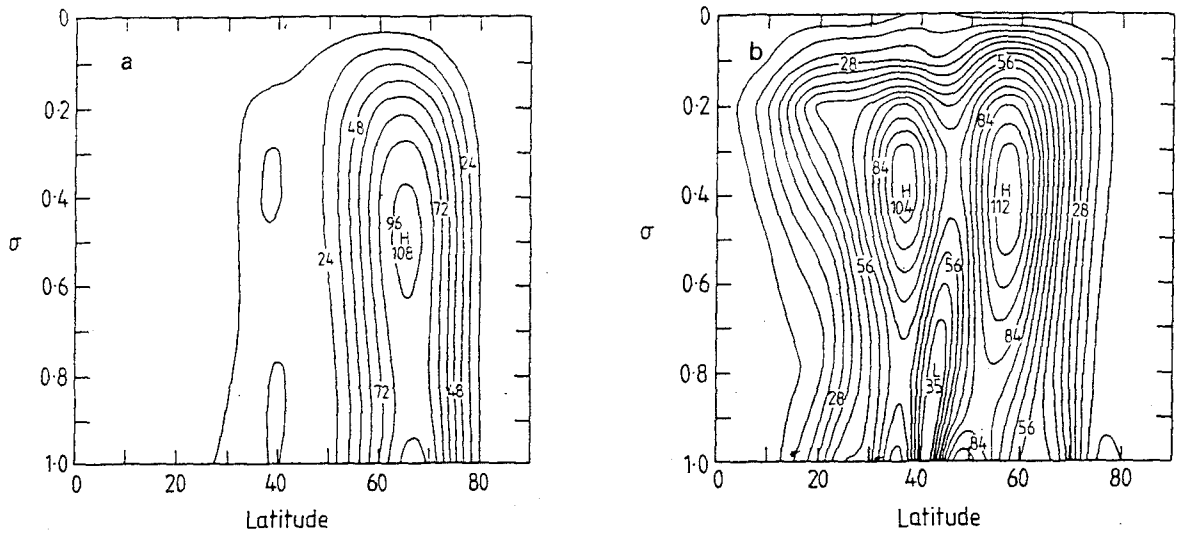

FIG. 4. Contribution to the eddy streamfunction amplitude for May from (a) $m = 5$ at day 11 and (b) $m = 5$ at day 15 in units of 10^4 m^2 s^{-1}.

also note that the penetration into the upper troposphere and the latitudinal spread is an improvement over the $m = 10$ nonlinear results shown in Fig. 11 of F2 for the same May basic state.

b. Eddy momentum fluxes

At day 6, the eddy momentum flux contribution from the dominant zonal wave number $m = 5$ is centered on 70° latitude and is practically purely equatorward with largest amplitude at the surface. Then by day 11 a poleward component of the flux has appeared whose center is located at $\sigma = 0.4$ and 58° latitude as shown in Fig. 5a. As the disturbance grows on the subtropical jet the centers of both the poleward and equatorward components move equatorward and the maximum amplitudes occur in the upper troposphere rather than at the surface as shown for day 15 in Fig. 5b.

By day 15, the comparison with the observed momentum flux for March–May in Fig. 4.9 of Newell *et al.* (1972) is quite reasonable. In fact, as expected, it is somewhat better than for the $m = 10$ wave growing on the same May zonal flow considered in F2.

c. Eddy heat fluxes

Again, by day 6 the eddy heat flux is qualitatively very similar to that of mode A with $m = 5$ discussed in F1 being practically purely poleward with maxi-

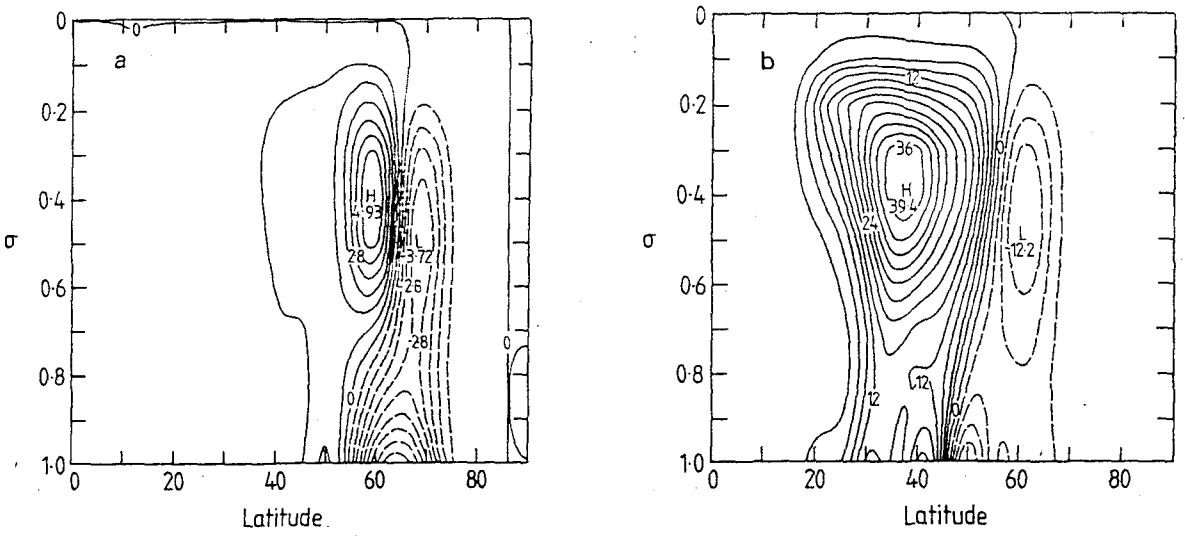

FIG. 5. Contribution to the zonally averaged eddy momentum flux for May by the rotational component of the wind $\overline{u_r v_r}\cos^2\phi$ in m^2 s^{-2} from (a) $m = 5$ at day 11 and (b) $m = 5$ at day 15.

Unauthenticated | Downloaded 02/23/24 11:48 PM UTC

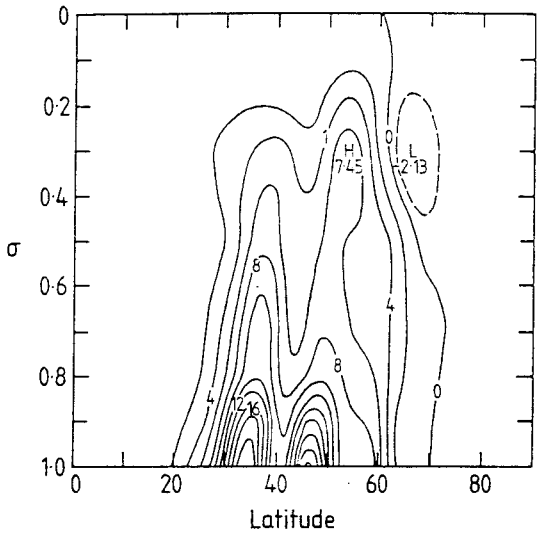

FIG. 6. Contribution to the zonally averaged eddy heat flux for May by the rotational component of the wind $\overline{v_r T}\cos\phi$ in K m s^{-1} from $m = 5$ at day 15.

mum amplitude at the surface centered at 70° latitude. Then during the integration it extends further into the troposphere and moves equatorward to latitude 60° by day 11. At this stage the beginnings of a secondary subsidiary maximum at $\sigma = 0.3$ also appears. Finally, by day 15 the heat flux has the appearance shown in Fig. 6 with two surface maxima at 34 and 46° and a secondary maximum at $\sigma = 0.3$ and latitude 52°. At this stage the qualitative comparison with Table 7.2 of Newell *et al.* (1972) for March to May is reasonable except that the upper level maximum in Fig. 6 is too weak.

d. Changes in the mean zonal wind

In this case the change in the maximum zonal wind at the subtropical and polar jets is much less dramatic from the January flow destabilized by a zonal wavenumber $m = 7$ disturbance (Fig. 9 of F2) and even less noticeable than that discussed in Section 5d. The polar jet maximum wanders only slightly about an average value of 52 m s^{-1} throughout the 15-day period while the subtropical jet increases slightly in strength from 35 to 37.5 m s^{-1}.

7. Kinetic energy spectra

In this section we examine in some detail the kinetic energy spectra for the January case at various stages of the evolution of the flow. Fig. 7 shows the vertically integrated kinetic energy spectrum $K(m)$ as a function of zonal wavenumber m at days 23, 50 and 55. Here day 23 corresponds to the time when wavenumber $m = 7$ reaches its maximum, day 50 is the last day of the viscous integration and day 55 is the last day of the 5-day inviscid integration shown in Fig. 1a. Also shown in Fig. 7 are lines corresponding to m^{-1}, m^{-3} and m^{-5} spectra.

We see that on day 23 the spectrum has a power law between -3 and -5, principally due to the large peak of energy in wavenumber $m = 7$. In fact, at this stage of the integration the qualitative appearance and power law of the spectrum is quite similar to that in Fig. 10 of Gall *et al.* (1979) for their Experiment 1. Their experiment was carried out in a grid point model with small perturbations growing on a zonally averaged Northern Hemisphere flow. The methodology was very similar to that described here in that their Experiment 1 was unforced although they also included surface friction.

For the present January Southern Hemisphere experiment the integration was continued with viscosity present [as given in the parameterizations (2.8)–(2.12) of F2] until day 50 by which time a statistical quasi-steady state[3] has been reached. An indication of this fact may be gained from Fig. 1a

[3] Since the model used here contains viscous dissipation an equilibrium solution will not be reached. Rather the system gradually loses energy; if this loss of energy is sufficiently slow, as is the case here, then a statistical quasi-steady state may be reached. It should be noted that there is considerable confusion over the use of equilibrium solution in the literature.

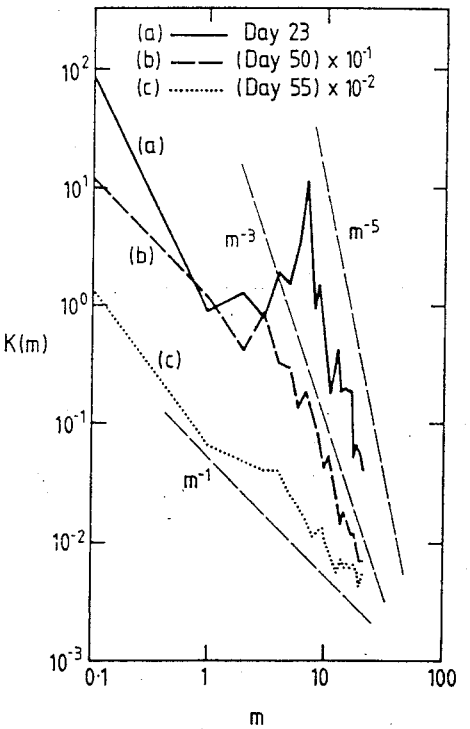

FIG. 7. Total vertically averaged kinetic energy spectra as a function of zonal wavenumber m on days 23, 50 and 55. Also shown are the power laws m^{-1}, m^{-3} and m^{-5}. The kinetic energy at $m = 0$ has been plotted at $m = 0.1$.

Unauthenticated | Downloaded 02/23/24 11:48 PM UTC

which shows that after day 45 the spectrum is an approximately monotonic decreasing function of m. At this stage the kinetic energy spectrum at day 50 (and also for a time average over the previous 5–10 days) has a power law which is approximately m^{-3}. This is consistent with the results of two-dimensional turbulence theory (Kraichnan,. 1967) and quasi-geostrophic turbulence theory (Charney, 1971) which predict a -3 power law for statistical steady states. It should also be noted that for systems which are not at a statistical steady state the spectrum depends on the initial conditions and may be practically anything depending on the initial preparation of the system and on how much time has elapsed. Comparing the present results with those of Gall *et al.* (1979) it would seem to the author that their Experiment 1 was not integrated for long enough to obtain a statistical quasi-steady state and that this is the reason for their -5 day power law and their disagreement with classical two-dimensional turbulence and quasi-geostrophic turbulence theory.

When the model was integrated for a further 5 days with no viscosity present the spectrum became flatter and at day 55 has a power law which is approximately m^{-1}. This is precisely the power law for inviscid two-dimensional turbulence as discussed for the case of the spherical nondivergent barotropic model by Frederiksen and Sawford (1980). In fact, by this stage of the integration the zonal flow has increased at the surface and the flow is effectively equivalent barotropic. Thus, it might be expected that the m^{-1} spectrum reflects the fact that the *rotational* part of the energy is trying to achieve an essentially barotropic statistical mechanical equilibrium of the type discussed in Frederiksen and Sawford (1980). In order to examine this in some more detail, we took the streamfunction at each level of the nine-level model and worked out the equilibrium statistical mechanical expectation values of the *rotational* energy and its variance that would result if the streamfunction were used to initialize an inviscid integration of the spherical nondivergent barotropic model. Both the viscous spectra at day 50 and the inviscid spectra at day 55 were compared with the (inviscid) equilibrium statistical mechanical expectation values.

For days 50 and 55, respectively, Figs. 8a and 8b and 9a and 9b show the rotational kinetic energy spectra $E(m)$ and $e(n)$ at the sigma level of 0.189 and as well the equilibrium expectation values of $E(m)$, $E(m) \pm \Sigma(m)$, $e(n)$ and $e(n) \pm \sigma(n)$. We recall that n is the total wavenumber and m the zonal wavenumber associated with the Legendre function P_n^m. Here $E(m)$ [respectively, $e(n)$] is obtained by summing the rotational kinetic energy over n (respectively m). Also, $\Sigma(m)$ is the standard deviation of the rotational energy $E(m)$ and $\sigma(n)$ of the rotational energy $e(n)$. The equilibrium expectation values in Fig. 8 (respectively Fig. 9) were calculated using the day 50 (respectively day 55) total rotational kinetic energy and the enstrophy as described in Frederiksen and Sawford (1980).

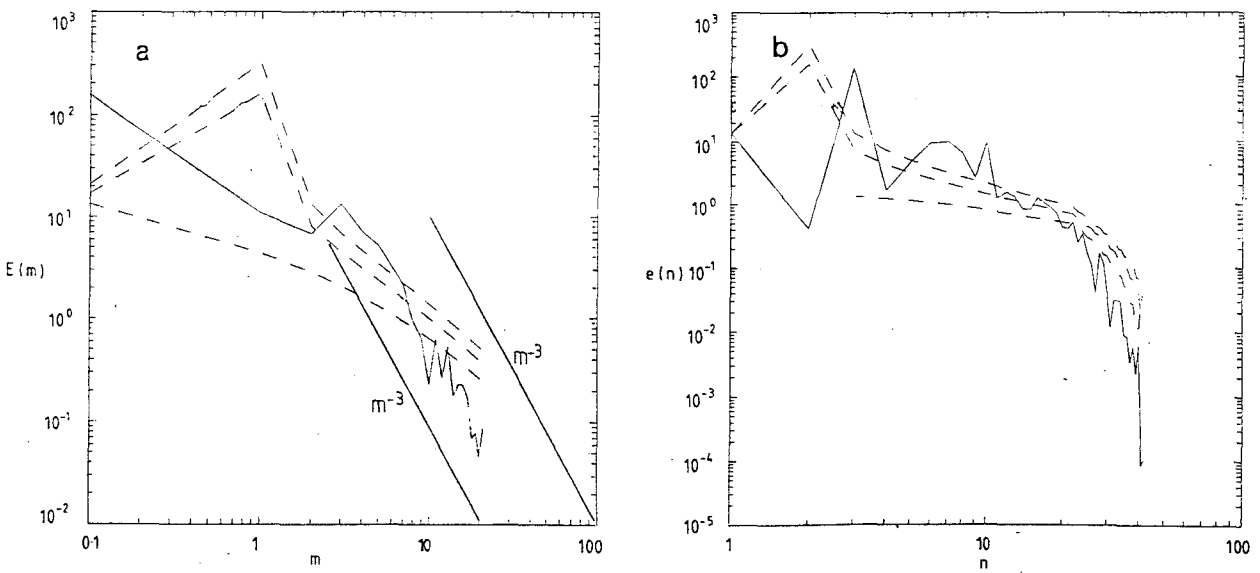

FIG. 8. (a) Kinetic energy spectrum $E(m)$ at $\sigma = 0.189$ on day 50 (light solid curve) as a function of zonal wavenumber m. Also shown are the statistical mechanical equilibrium expectation values of $E(m)$ and $E(m) \pm \Sigma(m)$ (dashed curves) and the power law m^{-3} (bold solid curves). The kinetic energy at $m = 0$ has been plotted at $m = 0.1$. (b) Kinetic energy spectrum $e(n)$ at $\sigma = 0.189$ on day 50 (solid curve) as a function of total wavenumber n. Also shown are the statistical mechanical equilibrium expectation values of $e(n)$ and $e(n) \pm \sigma(n)$ (dashed curves).

Unauthenticated | Downloaded 02/23/24 11:48 PM UTC

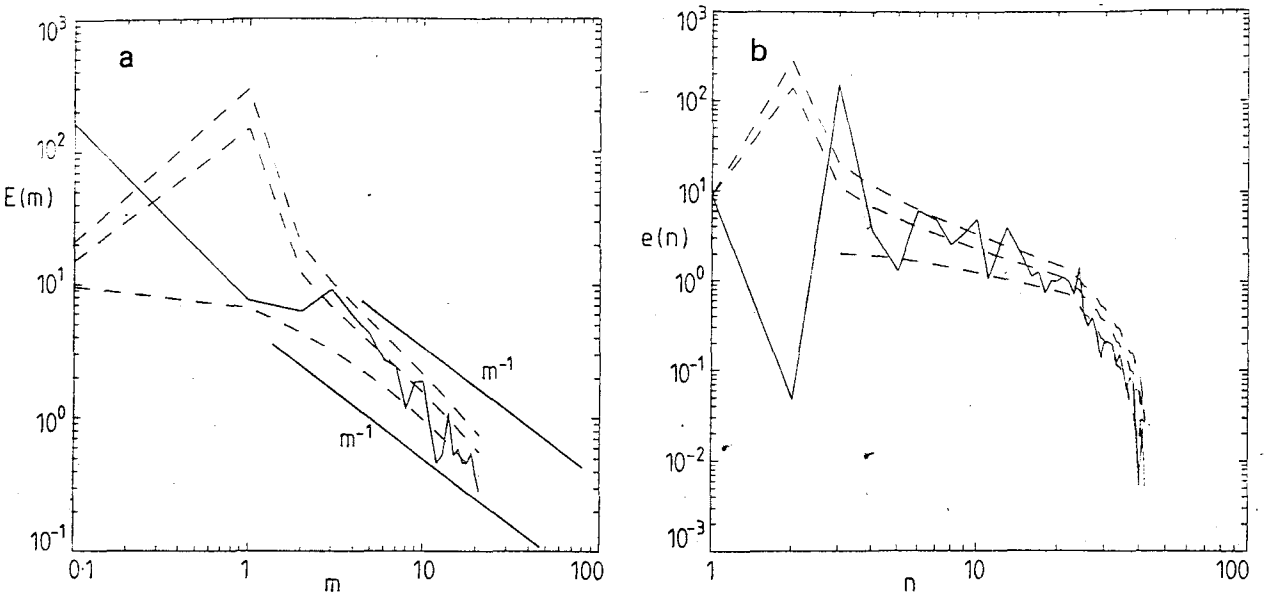

FIG. 9. (a) As in Fig. 8(a) except on day 55 and showing the power law m^{-1}. (b) As in Fig. 8(b) except on day 55.

As expected, for the viscous case, there is considerable deviation from the equilibrium values, particularly at small scales where the instantaneous spectra decrease more rapidly. In particular the model $E(m)$ spectrum has the m^{-3} power law of two-dimensional turbulence.

For the day 55 inviscid spectra the energy of most of the small and intermediate scales lie within one standard deviation of the equilibrium spectra indicating that the instantaneous field has spectra which are practically indistinguishable from those of one member of an equilibrium ensemble. We note that the $E(m)$ spectrum has an approximate m^{-1} behavior, although there is perhaps a systematic bias to slightly smaller values than the equilibrium values.

For both days 50 and 55 the qualitative behavior of the spectra at the other levels is similar to that described for the sigma level of 0.189.

It should be noted that the present results were obtained in a model without convective adjustment and that without viscosity present the static stability parameter eventually becomes negative at some places in the fluid. This became a problem shortly after day 55 and soon after day 58 the integration became computationally unstable.

Currently long-time integrations of inviscid shallow-water models and multilevel primitive equation spectral models with convective adjustment are being carried out with the view of studying their equilibrium properties. Since neither model conserves energy or potential enstrophy exactly, a theoretical (rather than numerical) analysis of the equilibrium properties is difficult. Similar problems recently have been considered by Carnevale and Frederiksen (1981) who comapre the equilibrium properties of inviscid nonlinear internal gravity waves and of Rossby waves with the corresponding equilibrium properties of these respective waves in their resonant interaction limit. For each class of waves an additional invariant exists in the resonant interaction limit and the equilibrium spectra therefore differ from those of the general primitive equations. The question then arises as to what will be the behavior of systems whose initial spectra are prepared to be realizations of the resonant interaction equilibrium spectra and for which the off-resonant interactions are small (but nonzero) compared with the resonant interactions. For such systems one would expect that the resonant interaction equilibrium spectra would be stable on a short time scale but on a long time scale the systems would move to the equilibrium spectra of the primitive equations.

For the shallow water integrations started with realistic initial fields, preliminary results indicate that the rotational part of the kinetic energy of the short scales approaches an m^{-1} spectrum which appears to be relatively stable. For the multilevel primitive equation spectral model integrations with convective adjustment and started with realistic initial fields, preliminary results indicate that the rotational kinetic energy of the short scales approaches an m^{-1} spectrum on a time scale of the order of 5–10 days. Thereafter, the kinetic energy of the shorter scales increases and the spectra become increasingly flatter over the next 50 days.

Unauthenticated | Downloaded 02/23/24 11:48 PM UTC

Thus, whether the m^{-1} spectrum for the multilevel primitive equation model is significant or not is perhaps, at this stage, debatable.

8. Discussion and conclusions

The growth and nonlinear development of initial small-amplitude disturbances, having a complete spectrum of zonal wavenumbers, m, and growing on January and May Southern Hemisphere zonal flow basic states, has been studied using a primitive equation spectral model. We have concentrated here on the differences and new aspects of the behavior of the eddies from those of F2. There similar nonlinear studies were carried out in which, however, the initial disturbance had a single zonal wavenumber. In the present study it is found that while individual zonal wavenumber contributions do exhibit vacillation cycles, the total eddy kinetic energy is, after the initial exponential growth, relatively constant, unlike the case of F2. We note that Yoden (1979, 1981) also has recently studied vacillation cycles in a two-level beta plane model.

For the January flow, during the initial period of almost exponential growth, the fastest growing mode is dominated by $m = 9$. This is quite close to the $m = 10$ found for the fastest growing mode in the linear instability study of F1, using the same basic state. However, after the barotropic decay of the $m = 9$ scale, the scale with $m = 7$ reaches its maximum amplitude which exceeds that of $m = 9$. Moveover, it is largely responsible for the agreement between the present results and observations. Thus, while linear theory is reasonably successful in predicting the fastest growing disturbance, the most important contributions to the eddy and fluxes, in the nonlinear regime, come from a somewhat smaller wavenumber.

For May, during the initial period of exponential growth, the disturbance is dominated by wavenumber $m = 5$, growing on the polar jet. This is in contrast with the linear inviscid results of F1 where the growth rate maximum occurs at $m = 10$. Nevertheless, the growth rate at $m = 5$ in the linear case is comparable with that at $m = 10$, unlike the January case. This would seem to be the reason why the introduction of viscous (and nonlinear) effects can produce such a large shift in the growth rate maximum.

On studying the disturbance streamfunction and eddy fluxes, we find that, although the fastest scale has $m = 9$ for January, the contribution from $m = 7$, at its peak, exceeds that of $m = 9$. Moreover, as far as the perturbation streamfunction is concerned, in order to obtain reasonable agreement with observations, it is necessary to take an average which includes the $m = 7$ scale with its maximum amplitude in the upper troposphere. Similarly, the $m = 7$ scale plays the most important role in achieving reasonable agreement with observations for eddy momentum and heat fluxes.

For May, the disturbance, dominated by $m = 5$, initially starts growing on the polar jet near the surface. However, by day 11 the amplitude at $\sigma = 0.5$ equals that at the ground and growth is commencing on the subtropical jet. By day 15, the disturbance has significant amplitude in the upper troposphere in the latitude band between 30 and 60 degrees. Thus, we have here a case of a disturbance being triggered in the poleward regions and subsequently developing further in midlatitudes by growing on the subtropical jet. The momentum flux in the early stages of growth is purely equatorward and centered near 70° latitude. By day 11 in the upper troposphere a poleward component has developed which by day 15 dominates the flux and is centered at midlatitudes. At this stage the momentum flux compares favorably with observations. Again, by day 15, the eddy heat flux is in reasonably good agreement with observations, although the penetration into the troposphere is somewhat less than observed.

For the January flow case, the integrations were continued past the periods of barotropic decay of the $m = 9$ and $m = 7$ scales out to day 50. At this stage the viscosity was switched off and the integration carried on for a further 5 days. Kinetic energy spectra were calculated at day 23, when the energy at $m = 7$ was a maximum, at day 50, when a statistical quasi-steady state was arrived at, and at day 55. At day 23, the kinetic energy spectrum has a rather steep power law of approximately m^{-5}, while by day 50 the m^{-3} power law of classical two-dimensional and quasi-geostrophic turbulence applies. At day 55, an m^{-1} power law was obtained.

Acknowledgments. It is a pleasure to thank W. Bourke, B. McAvaney, K. Puri and R. Thurling for informative discussions on spectral models and for making available their model. I am grateful to A. Kasahara and C. E. Leith for their hospitality during a visit to NCAR. The assistance of A. G. Davies in modifying parts of the spectral model and the help of H. Rabich in developing contour plotting routines are greatly appreciated. I wish to thank P. Nelson for drawing the graphs and L. Heumiller for typing the manuscript.

REFERENCES

Bourke, W., 1974: A multi-level spectral model. I. Formulation and hemispheric integrations. *Mon. Wea. Rev.*, **102**, 687–701.

——, B. McAvaney, K. Puri and R. Thurling, 1977: Global modelling of atmospheric flow by spectral methods. *Methods Comput. Phys.*, **17**, 267–324.

Unauthenticated | Downloaded 02/23/24 11:48 PM UTC

Carnevale, G. F., and J. S. Frederiksen, 1981: A statistical dynamical theory of strongly nonlinear internal gravity waves. Submitted to *Geophys. Astrophys. Fluid Dyn.*

Charney, J. G., 1971: Geostrophic turbulence. *J. Atmos. Sci.*, **28**, 1087–1093.

Daley, R., and K. Puri, 1980: Four-dimensional data assimilation and the slow manifold. *Mon. Wea. Rev.*, **108**, 85–99.

Frederiksen, J. S., 1981a: Disturbances and eddy fluxes in Southern Hemisphere flows: Linear theory. *J. Atmos. Sci.*, **38**, 673–689.

——, 1981b: Growth and vacillation cycles of disturbances in Southern Hemisphere flows. *J. Atmos. Sci.*, **38**, 1360–1375.

——, and B. L. Sawford, 1980: Statistical dynamics of two-dimensional inviscid flow on a sphere. *J. Atmos. Sci.*, **37**, 717–732.

Gall, R., R. Blakeslee and R. C. J. Somerville, 1979: Baroclinic instability and the selection of zonal scale of transient eddies of middle latitudes. *J. Atmos. Sci.*, **36**, 767–784.

Kraichnan, R., 1967: Inertial ranges in two-dimensional turbulence. *Phys. Fluids*, **10**, 1417–1423.

Machenhauer, B., 1977: On the dynamics of gravity oscillations in a shallow water model, with application to normal mode initialization. *Beitr. Phys. Atmos.*, **50**, 253–271.

McAvaney, B. J., W. Bourke and K. Puri, 1978: A global spectral model for simulation of the general circulation. *J. Atmos. Sci.*, **35**, 1557–1583.

Newell, R. E., J. W. Kidson, D. G. Vincent and G. J. Boer, 1972: *The General Circulation of the Tropical Atmosphere and Interactions with Extratropical Latitudes*, Vol. 1. MIT Press, 258 pp.

——, ——, —— and ——, 1974: *The General Circulation of the Tropical Atmosphere and Interactions with Extratropical Latitudes*, Vol. 2. MIT Press, 371 pp.

Simmons, A. J., and B. J. Hoskins, 1976: Baroclinic instability on the sphere: Normal modes of the primitive and quasi-geostrophic equations. *J. Atmos. Sci.*, **33**, 1454–1477.

Yoden, S., 1979: Some dynamical properties of nonlinear baroclinic waves in a quasi-geostrophic model. *J. Meteor. Soc. Japan*, **57**, 493–504.

——, 1981: Quasi-periodic energy variation in a zonal flow baroclinic wave interaction model. *J. Meteor. Soc. Japan* (in press).

Unauthenticated | Downloaded 02/23/24 11:48 PM UTC